Solar Cells

International Edition: DOI: 10.1002/anie.201411329
German Edition: DOI: 10.1002/ange.201411329

$CuSbS_2$-Sensitized Inorganic–Organic Heterojunction Solar Cells Fabricated Using a Metal–Thiourea Complex Solution**

*Yong Chan Choi, Eun Joo Yeom, Tae Kyu Ahn, and Sang Il Seok**

Abstract: *The device performance of sensitizer-architecture solar cells based on a $CuSbS_2$ light sensitizer is presented. The device consists of F-doped SnO_2 substrate/TiO_2 blocking layer/mesoporous TiO_2/$CuSbS_2$/hole-transporting material/Au electrode. The $CuSbS_2$ was deposited by repeated cycles of spin coating of a Cu-Sb-thiourea complex solution and thermal decomposition, followed by annealing in Ar at 500°C. Poly(2,6-(4,4-bis-(2-ethylhexyl)-4H-cyclopenta[2,1-b;3,4-b′]dithiophene)-alt-4,7(2,1,3-benzothiadiazole)) (PCPDTBT) was used as the hole-transporting material. The best-performing cell exhibited a 3.1 % device efficiency, with a short-circuit current density of 21.5 mA cm^{-2}, an open-circuit voltage of 304 mV, and a fill factor of 46.8 %.*

Binary antimony chalcogenides (Sb-Ch), such as Sb_2S_3,[1,2] Sb_2Se_3,[3,4] and composition-graded $Sb_2(S/Se)_3$,[5] have been successfully applied as light absorbers in both sensitizer-architecture and planar-type solar cells because of their specific properties, such as suitable band gaps of 1.1–1.7 eV, chemical stability, high absorption coefficients, and environmentally friendly characteristics.[1–7] Theoretical and experimental investigations on solar cells based on Sb-Ch have shown their potential as light absorbers.[1–4,7] For example, we recently achieved a record power conversion efficiency (PCE) of about 7.5 % in Sb_2S_3-sensitized solar cells through thioacetamide-assisted surface treatment of Sb_2S_3.[2d] However, despite the promising solar cell characteristics, Sb-Ch solar cells still suffer from a limited device efficiency of less than 10 %, owing to efficient recombination centers in Sb-Ch and a dominant energy-loss channel caused by strong electron–phonon interactions.[2d,8–10]

To overcome these limitations, we have explored alternative chalcogenides that have characteristics comparable to those of Sb-Ch. Among the various chalcogenides, ternary $CuSbS_2$ chalcogenide (chalcostibite) has significant potential as a promising light absorber because it has a layered orthorhombic structure with a *Pnma* space group, a high absorption coefficient of 10^5 cm^{-1}, and a bandgap of 1.5–1.7 eV.[11,12] Furthermore, this material exhibits p-type semiconductor behavior with an electrical mobility of up to 20 cm^2 V^{-1} S^{-1},[12] which may provide an additional driving force for hole transfer from the light absorber to the hole-transporting material (HTM). Theoretical investigations performed by Yu et al. showed that $CuSbS_2$ planar solar cells may be able to exhibit higher device performance than $CuInSe_2$ planar cells owing to the better electrical and optical properties of $CuSbS_2$ than $CuInSe_2$.[11b] Several groups experimentally demonstrated the device performance of $CuSbS_2$ planar-type solar cells, which showed a maximum PCE of 3.13 %.[11d,e,13] Although this material has not yet been applied to sensitizer-architecture solar cells, it can be used as a light sensitizer in such devices because of the well-matched energy levels of $CuSbS_2$ to the photoelectrode and HTM (Supporting Information, Figure S1).

$CuSbS_2$ has been prepared by several methods, such as sequential chemical bath deposition (CBD) of CuS/Sb_2S_3,[13] the hot-injection method,[11c] sulfurization of metallic stacks of Cu/Sb,[11d] a hydrazine-based solution process,[11e] and a thiol/amine-based solution approach.[14] Among the various methods, the solution processing method is particularly suitable for low-cost, high-throughput deposition of $CuSbS_2$ onto the desired substrates. Furthermore, solution processing is very useful for controlling the Cu/Sb ratio by applying appropriate amounts of Cu/Sb chemicals; it is critical to control the ratio of Cu/Sb for the formation of a pure $CuSbS_2$ phase.[11e] However, the solution methods reported to date have some limitations. For example, in case of the sequential CBD method, precise control of the thickness ratio of CuS and Sb_2S_3 is required to obtain stoichiometric $CuSbS_2$.[13] On the other hand, the hydrazine-based approach suffers from the inevitable usage of hydrazine, which is an extremely toxic and explosive solvent. Therefore, it is highly desirable to develop a simple, low-toxic, and versatile solution approach to fabricate high-efficiency $CuSbS_2$ solar cells.

In this work, we report the fabrication of high-quality $CuSbS_2$ by simple and low-toxic solution processing and its application to sensitizer-architecture solar cells composed of fluorine-doped SnO_2 (FTO)/TiO_2 blocking layer (BL-TiO_2)/mesoporous TiO_2 (mp-TiO_2) + $CuSbS_2$ light sensitizers/HTM/Au. We developed a simple chemical route based on a metal–thiourea complex solution for the fabrication of $CuSbS_2$. For

[*] Dr. Y. C. Choi, Prof. S. I. Seok
Division of Advanced Materials
Korea Research Institute of Chemical Technology (KRICT)
141 Gajeong-Ro, Yuseong-Gu, Daejeon 305-600 (Republic of Korea)
E-mail: seoksi@krict.re.kr
E. J. Yeom, Prof. T. K. Ahn, Prof. S. I. Seok
Department of Energy Science, Sungkyunkwan University
Suwon 440-746 (Republic of Korea)
E-mail: seoksi@skku.edu

[**] This study was supported by the Global Research Laboratory (GRL) Program and the Global Frontier R&D Program on Center for Multiscale Energy System funded by the National Foundation under the Ministry of Science, ICT & Future, Korea, and by a grant from the KRICT 2020 Program for Future Technology of the Korea Research Institute of Chemical Technology (KRICT), Republic of Korea.

Supporting information for this article is available on the WWW under http://dx.doi.org/10.1002/anie.201411329.

the synthesis, we used highly soluble, inexpensive metal precursors and non-hydrazine organic solvents. The $CuSbS_2$ was deposited onto FTO/BL-TiO_2/mp-TiO_2 by repeated cycles of spin coating of a copper–antimony–thiourea complex solution and subsequent thermal decomposition. The structure, morphology, and absorption properties of the as-prepared $CuSbS_2$ were characterized by X-ray diffraction (XRD) patterns, field-emission scanning electron microscopy (FESEM), and UV/Vis absorption spectra, respectively.

Figure 1 a shows the XRD patterns of the powders of the copper–antimony–thiourea complex solution annealed at

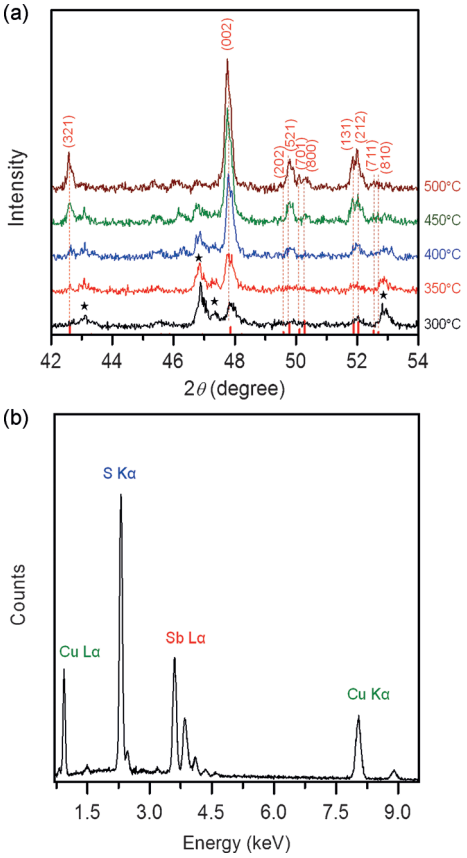

Figure 1. a) XRD patterns of the powders annealed at temperatures of 300–500 °C in Ar. b) EDX spectrum of the powder annealed at 500 °C.

300–500 °C in Ar. Two mixed phases of Sb_2S_3 (denoted by black stars, JCPDS No. 42-1393) and $CuSbS_2$ (denoted by red dotted lines, JCPDS No. 44-1427) are detected at a temperature of 300 °C. The Sb_2S_3 phase gradually decreases, whereas the $CuSbS_2$ phase steadily increases as the temperature increases, and a pure $CuSbS_2$ phase is finally obtained at 500 °C. To further confirm this material, the chemical composition of the sample annealed at 500 °C was evaluated by energy-dispersive X-ray (EDX) spectroscopy (Figure 1 b). The atomic ratio of Cu/Sb/S was measured as 1.1:1.0:2.2, which is very close to the stoichiometric value of 1:1:2. Detailed structural and compositional changes as a function of annealing temperature are shown in the Supporting Information, Figure S2 and Table S1. These results indicate that our copper–antimony–thiourea precursor solution can be used to deposit $CuSbS_2$ for application in solar cells.

To apply the $CuSbS_2$ as the light sensitizer in sensitizer-architecture solar cells, we first deposited it on FTO/TiO_2-BL/mp-TiO_2 substrates by repeated cycles of spin coating of a diluted precursor solution and thermal decomposition at 200 °C (Figure 2 a). Note that the thermal decomposition

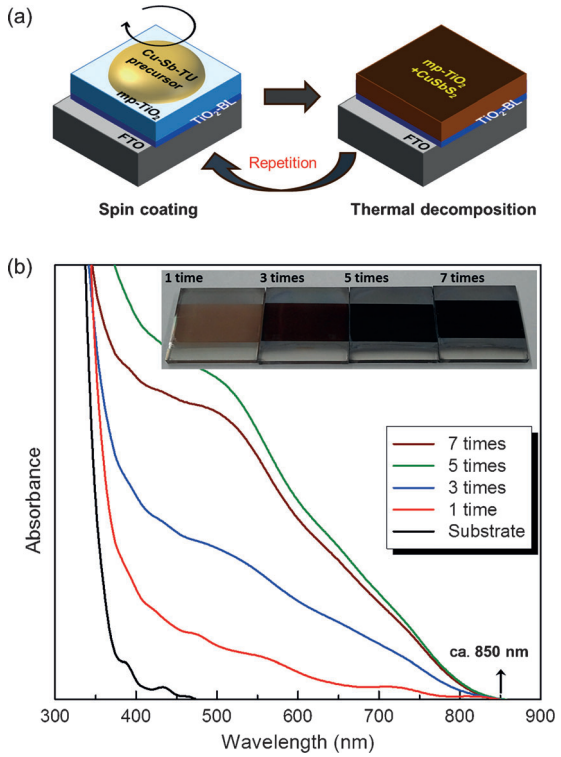

Figure 2. a) The $CuSbS_2$ deposition process on mp-TiO_2/TiO_2-BL/FTO substrate using metal–thiourea complex precursor solution for solar cell applications. b) UV/Vis absorption spectra and corresponding photographs (inset images) of $CuSbS_2$/mp-TiO_2/TiO_2-BL/FTO fabricated with varying numbers of cycles and the mp-TiO_2/TiO_2-BL/FTO substrate.

process is necessary as part of these repeated cycles because the thermally decomposed precursor becomes insoluble in the parent solvent, which makes possible repeated deposition of $CuSbS_2$. Also, the thermal decomposition process must be performed in an inert atmosphere (either Ar or N_2) to prevent formation of other secondary phases such as metal oxides (Supporting Information, Figures S3 and S4, Table S2). The repeated cycles allowed us to precisely control the amount of $CuSbS_2$. After repeated deposition of $CuSbS_2$, the samples were finally annealed at 500 °C in Ar to form a single $CuSbS_2$ phase. Figure 2 b shows the UV/Vis absorption spectra of FTO/TiO_2-BL/mp-TiO_2 + $CuSbS_2$ as a function of the number of deposition cycles. The $CuSbS_2$ absorption gradually increases as the number of deposition cycles increases to five times and it slightly decreases at seven times cycles. This implies that each cycle increases the amount of $CuSbS_2$ but more than seven cycles are not necessary for sufficient light absorption. All samples exhibit an absorption edge of about

850 nm, indicating that the as-deposited $CuSbS_2$ has a band gap of about 1.5 eV.

The $CuSbS_2$ distribution inside the mp-TiO_2 was investigated by observing the morphology and elemental composition by FESEM equipped with an EDX spectrometer. The $CuSbS_2$ was deposited by using five cycles of spin coating and thermal decomposition, followed by annealing at 500 °C in Ar. As shown in FESEM surface images (Figure 3a, left), the morphology of the surface of FTO/TiO_2-BL/mp-TiO_2 + $CuSbS_2$ is very similar with that of the surface without $CuSbS_2$, that is, the mp-TiO_2 surface, except for the particle sizes. This indicates the uniform distribution of $CuSbS_2$ on the surface of mp-TiO_2. The EDX line scan profile (Figure 3b) with elemental mapping data (Figure 3c) further confirms the uniform distribution of $CuSbS_2$ across the surface of mp-TiO_2.

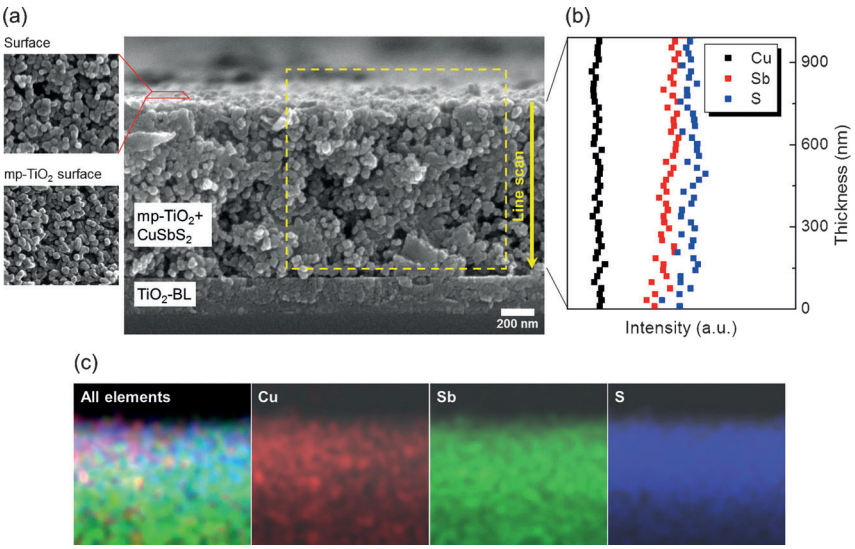

Figure 3. a) Surface and cross-sectional FESEM images of $CuSbS_2$/mp-TiO_2/TiO_2-BL/FTO fabricated through metal–thiourea complex solution processing. b) EDX line scan profile through the mp-TiO_2 depth and c) EDX elemental mapping images for the dotted yellow area in (a).

Figure 4a shows photocurrent density–voltage (J–V) curves for solar cells fabricated with and without poly-{(2,6-(4,4-bis-(2-ethylhexyl)-4*H*-cyclopenta[2,1-*b*;3,4-*b*′]dithiophene)-alt-4,7(2,1,3-benzothiadiazole))} (PCPDTBT) as a HTM. All device performances are summarized in Table 1. In these devices, $CuSbS_2$ was deposited with the same conditions as those of the samples shown in Figure 3. The cells without HTM exhibited a PCE of about 1%, with a short-circuit current density (J_{SC}) of 11.7 mA cm^{-2}. This result indicates that the $CuSbS_2$ acts not only as an efficient light absorber but also as a hole transporter. The hole-transporting property of $CuSbS_2$ may be attributed to its intrinsic p-type nature caused by dominant Cu vacancies.[11e] After HTM deposition, the device efficiency increased to 1.4% because of a significant increase of J_{SC} from 11.7 to 18.2 mA cm^{-2}. The increase of HTM concentration induces further enhancement of PCE to 2.6% with increasing open-circuit voltage (V_{OC}) from 187.0 to 272.0 mV while maintaining J_{SC}. To elucidate the reasons behind the effect of HTM on the performance variation, we investigated the corresponding incident-photon-to-current-efficiency (IPCE) spectra, which are closely linked to J_{SC}. The IPCE is generally determined by the light-harvesting efficiency (LHE) and electron-transfer yield (Φ_{ET}), where Φ_{ET} is defined as the product of the electron injection yield and charge collection efficiency. As $CuSbS_2$ is equally deposited for all samples, all samples should have the same LHE. Thus, the IPCE variations with corresponding similar J_{SC} changes can be explained by the different behaviors of Φ_{ET}. In the current device system, the surface effects of $CuSbS_2$ may be significant owing to the high surface-area-to-volume ratio because the $CuSbS_2$ is deposited in the form of an extremely thin layer on the mp-TiO_2 surface. These morphological features make the surfaces

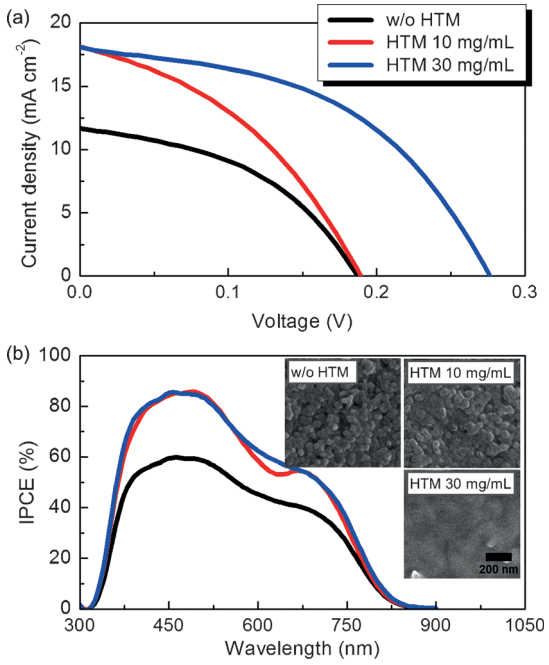

Figure 4. a) J–V curves and b) IPCE spectra of the $CuSbS_2$-sensitized solar cells with and without PCPDTBT. Inset images in (b) are the corresponding FESEM surface images of the cells.

Table 1: Summary of device parameters shown in Figure 4.

	J_{SC} [mA cm^{-2}]	V_{OC} [mV]	FF [%]	PCE [%]
without PCPDTBT	11.7	187.0	43.8	1.0
PCPDTBT 10 mg mL^{-1}	18.2	187.0	39.4	1.4
PCPDTBT 30 mg mL^{-1}	18.1	272.7	48.1	2.6

prone to form defects as dominant recombination centers, which may result in a significant decrease of Φ_{ET}, that is, a low IPCE, as well as a low J_{SC}. After the HTM deposition, the backward transport of electrons toward the Au electrode may be blocked because the lowest-unoccupied-molecular-orbital (LUMO) level of PCPDTBT (3.6 eV) is higher than the conduction band edge (3.85 eV) of $CuSbS_2$. Furthermore, the highly porous surfaces become denser by pore filling with HTM (Figure 4b, insets). In such a dense structure, not only do the interactions at each interface become stronger but also direct contact between mp-TiO_2 and the Au electrode is restricted, which improves Φ_{ET} and reduces recombination in the samples with HTM. As a result, both J_{SC} and V_{OC} can be simultaneously increased after the proper concentration of HTM is deposited on the $CuSbS_2$ surface. It is noted that a further increase of HTM concentration ($>30\,mg\,mL^{-1}$) causes low J_{SC} with high series resistances, leading to lower PCE. Similar behaviors have also been observed in solid-state dye-sensitized solar cells utilizing spiro-OMeTAD (2,2′,7,7′-tetrakis-(*N*,*N*-di-*p*-methoxyphenylamine)9,9′-spirobifluorene).[15] However, further studies are needed to confirm the effects of pore filling with HTM and the interaction between $CuSbS_2$ and HTM on device performance.

To further enhance the device performance of the cells, we tested many experimental parameters, such as mole concentrations of precursor sol, number of cycles for $CuSbS_2$ deposition, HTM concentration, and mp-TiO_2 thickness (Supporting Information, Figures S5–S7). Through such cell optimization and repeated fabrication, we obtained solar cells with optimum efficiency by using a 0.2–0.5 M precursor solution, 1000 nm-thick mp-TiO_2 with a 50 nm particle size, and a $30\,mg\,mL^{-1}$ PCPDTBT concentration in 1,2-dichlorobenzene. The *J*–*V* curve and IPCE spectrum of this best-performing solar cell are presented in Figure 5a and b, respectively. The device exhibits a J_{SC} of 21.5 mA cm^{-2}, a V_{OC} of 304.0 mV, and a fill factor (FF) of 46.8%, corresponding to a PCE of 3.12% under standard air-mass (AM) 1.5 G conditions.

This device also shows a very broad IPCE extended to about 850 nm, which is consistent with the absorption edge as shown in Figure 2b. The J_{SC} value of 19.4 mA cm^{-2} integrated from the IPCE spectrum is very close to that obtained from the *J*–*V* curve of Figure 5a. An additional histogram of PCE for the independently fabricated cells that contributed to the current study is presented in Figure 5c. We believe that the metal–thiourea precursor solution processing presented here provides a simple and versatile route for the fabrication of high efficiency metal chalcogenide-based solar cells because most metal salts can readily form metal–thiourea complexes in the presence of thiourea.[16,17] In comparison with the device performances reported to date,[11d,e,13] our device shows a lower V_{OC} of less than 0.4 V, despite the excellent photocurrents exceeding 20 mA cm^{-2}. One possible reason for the low V_{OC} may be the presence of many surface recombination centers resulting induced from the morphological features of $CuSbS_2$. This issue may be solved by surface-defect modulation/healing of $CuSbS_2$, such as defect-heating by post-sulfurization[11d] and systematic control of the Cu/Sb ratio.[11e] Determining the optimum HTM, which may have a strong chemical interaction with $CuSbS_2$, may also help improve the V_{OC} and the FF.[2c] Therefore, further study for improving V_{OC} is currently underway.

In summary, $CuSbS_2$ was successfully deposited onto FTO/TiO_2-BL/mp-TiO_2 by using simple metal–thiourea complex solution. The process consisted of two steps, namely spin coating of the precursor solution and thermal decomposition in Ar at 200 °C, followed by annealing at 500 °C in Ar. The precursor sol was synthesized by a reaction of metal chlorides with thiourea in organic solvents. The resulting device composed of FTO/TiO_2-BL/mp-TiO_2 + $CuSbS_2$ HTM/Au exhibited a comparable device efficiency of about 3.12% with a J_{SC} of 21.5 mA cm^{-2}. The $CuSbS_2$-sensitized device also showed a broad IPCE spectrum covering a wavelength region to about 850 nm.

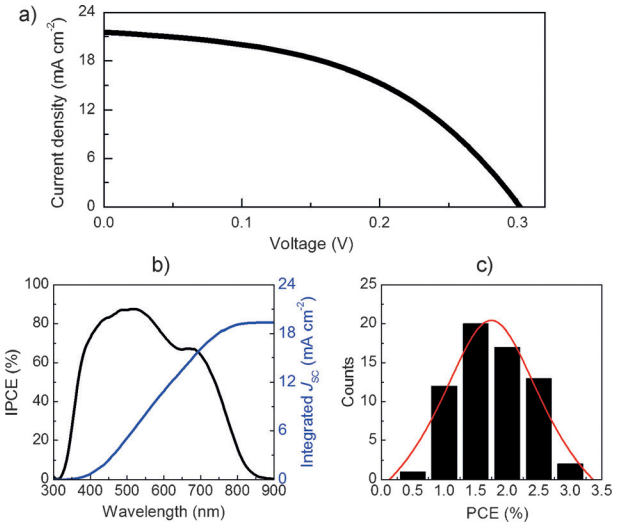

Figure 5. a) *J*–*V* curve and b) IPCE spectrum of the best-performing cells in our study. c) Histogram of device efficiencies from the 135 devices fabricated independently.

Keywords: antimony · copper · sensitizers · solar cells · thiourea

How to cite: *Angew. Chem. Int. Ed.* **2015**, *54*, 4005–4009
Angew. Chem. **2015**, *127*, 4077–4081

[1] a) Y. Itzhaik, O. Niitsoo, M. Page, G. Hodes, *J. Phys. Chem. C* **2010**, *113*, 4252; b) S.-J. Moon, Y. Itzhaik, J.-H. Yum, S. M. Zakeeruddin, G. Hodes, M. Gratzel, *J. Phys. Chem. Lett.* **2010**, *1*, 1524; c) K. Tsujimoto, D.-C. Nguyen, S. Ito, H. Nishino, H. Matsuyoshi, A. Konno, G. R. A. Kumara, K. Tennakone, *J. Phys. Chem. C* **2012**, *116*, 13465; d) S. Ito, K. Tsujimoto, D.-C. Nguyen, K. Manabe, H. Nishino, *Int. J. Hydrogen Energy* **2013**, *38*, 16749.

[2] a) J. A. Chang, J. H. Rhee, S. H. Im, Y. H. Lee, H.-J. Kim, S. I. Seok, *Nano Lett.* **2010**, *10*, 2609; b) S. H. Im, C.-S. Lim, J. A. Chang, Y. H. Lee, N. Maiti, H.-J. Kim, Md. K. Nazeeruddin, M. Grätzel, S. I. Seok, *Nano Lett.* **2011**, *11*, 4789; c) J. A. Chang, S. H. Im, Y. H. Lee, H.-J. Kim, C.-S. Lim, J. H. Heo, S. I. Seok, *Nano Lett.* **2012**, *12*, 1863; d) Y. C. Choi, D. U. Lee, J. H. Noh, E. K. Kim, S. I. Seok, *Adv. Funct. Mater.* **2014**, *24*, 3587.

[3] Y. C. Choi, T. N. Mandal, W. S. Yang, Y. H. Lee, S. H. Im, J. H. Noh, S. I. Seok, *Angew. Chem. Int. Ed.* **2014**, *53*, 1329; *Angew. Chem.* **2014**, *126*, 1353.

[4] a) T. T. Ngo, S. Chavham, I. Kosta, O. Miguel, H.-J. Grande, R. Tena-Zaera, *ACS Appl. Mater. Interfaces* **2014**, *6*, 2836; b) X. Liu, J. Chen, M. Luo, Z. Xia, Y. Zhou, S. Qin, D.-J. Xue, L. Lv, H. Huang, D. Niu, J. Tang, *ACS Appl. Mater. Interfaces* **2014**, *6*, 10687; c) Y. Zhou, M. Leng, Z. Xia, J. Zhong, H. Song, X. Liu, B. Yang, J. Zhang, J. Chem, K. Zhou, J. Han, Y. Cheng, J. Tang, *Adv. Energy Mater.* **2014**, *4*, 1301846.
[5] Y. C. Choi, Y. H. Lee, S. H. Im, J. H. Noh, T. N. Mandal, W. S. Yang, S. I. Seok, *Adv. Energy Mater.* **2014**, *4*, 1301680.
[6] M. Y. Versavel, J. A. Haber, *Thin Solid Films* **2007**, *515*, 7171.
[7] M. R. Filip, C. E. Patrick, F. Giustino, *Phys. Rev. B* **2013**, *87*, 205125.
[8] a) P. P. Boix, G. Larramona, A. Jacob, B. Delatouche, I. Mora-Sero, J. Bisquert, *J. Phys. Chem. C* **2012**, *116*, 1579; b) P. P. Boix, Y. H. Lee, F. Fabregat-Santiago, I. Mora-Sero, J. Bisquert, S. I. Seok, *ACS Nano* **2012**, *6*, 873; c) D. U. Lee, S. W. Park, S. G. Cho, E. K. Kim, S. I. Seok, *Appl. Phys. Lett.* **2013**, *103*, 023901.
[9] a) J. A. Christians, P. V. Kamat, *ACS Nano* **2013**, *7*, 7967; b) J. A. Christians, D. T. Veighton, Jr., P. V. Kamat, *Energy Environ. Sci.* **2014**, *7*, 1148.
[10] W. K. Chong, G. Xing, Y. Liu, E. L. Gui, Q. Zhang, Q. Sxiong, N. Mathews, C. K. Gan, T. C. Sum, *Phys. Rev. B* **2014**, *90*, 035208.
[11] a) D. J. Temple, A. B. Kehoe, J. P. Allen, G. W. Watson, D. O. Scanlon, *J. Phys. Chem. C* **2011**, *116*, 7334; b) L. Yu, R. S. Kokenyesi, D. A. Keszler, A. Zunger, *Adv. Energy Mater.* **2013**, *3*, 43; c) K. Ramasamy, H. Sims, W. H. Butler, A. Gupta, *Chem. Mater.* **2014**, *26*, 2891; d) W. Septina, S. Ikeda, Y. Iga, T. Harada, M. Matsumura, *Thin Solid Films* **2014**, *550*, 700; e) B. Yang, L. Wang, J. Han, Y. Zhou, H. Song, S. Chen, J. Zhong, L. Lv, D. Niu, J. Tang, *Chem. Mater.* **2014**, *26*, 3135.
[12] a) C. Garza, S. Shaji, A. Arato, E. P. Tijerina, G. A. Castillo, T. K. D. Roy, B. Krishnan, *Sol. Energy Mater. Sol. Cells* **2011**, *95*, 2001; b) W. Wubet, D.-H. Kuo, *Mater. Res. Bull.* **2014**, *53*, 290.
[13] Y. Rodríguez-Lazcano, M. T. S. Nair, P. K. Nair, *J. Electrochem. Soc.* **2005**, *152*, G635.
[14] Q. Tian, G. Wang, W. Zhao, Y. Chen, Y. Yang, L. Huang, D. Pan, *Chem. Mater.* **2014**, *26*, 3098.
[15] I.-K. Ding, N. Tetreault, J. Brillet, B. E. Hardin, E. H. Smith, S. J. Rosenthal, F. Sauvage, M. Gratzel, M. D. McGehee, *Adv. Funct. Mater.* **2009**, *19*, 2431.
[16] G. A. Bowmaker, J. V. Hanna, C. Pakawatchai, B. W. Skelton, Y. Thanysirikul, A. H. White, *Inorg. Chem.* **2009**, *48*, 350.
[17] I. I. Ozturk, N. Kourkoumelis, S. K. Hadjikakou, M. J. Manos, A. J. Tasiopoulos, I. S. Butler, J. Balzarini, N. Hadjiliadis, *J. Coord. Chem.* **2011**, *64*, 3859.

Received: November 24, 2014
Published online: February 3, 2015

